

ASSESSING THE RELATIONSHIP OF LST, NDVI AND EVI WITH LAND COVER CHANGES IN THE LAGOS LAGOON ENVIRONMENT

ALFRED S. ALADEMOMI , CHUKWUMA J. OKOLIE , OLAGOKE E. DARAMOLA ,
RAPHAEL O. AGBOOLA , TOSIN J. SALAMI 

Department of Surveying and Geoinformatics, Faculty of Engineering, University of Lagos, Lagos, Nigeria

Manuscript received: May 20, 2020

Revised version: August 19, 2020

ALADEMOMI A.S., OKOLIE C.J., DARAMOLA O.E., AGBOOLA R.O., SALAMI T.J., 2020. Assessing the relationship of LST, NDVI and EVI with Land Cover changes in the Lagos Lagoon environment. *Quaestiones Geographicae* 39(3), Bogucki Wydawnictwo Naukowe, Poznań, pp. 87–109. 13 figs, 12 tables.

ABSTRACT: The Lagos Lagoon is under increased pressure from growth in human population, growing demands for natural resources, human activities, and socioeconomic factors. The degree of these activities and the impacts are directly proportional to urban expansion and growth. In the light of this situation, the objectives of this study were: (i) to estimate through satellite imagery analysis the extent of changes in the Lagos Lagoon environment for the periods 1984, 2002, 2013 and 2019 using Landsat-derived data on land cover, Land Surface Temperature (LST), Normalised Difference Vegetation Index (NDVI) and Enhanced Vegetation Index (EVI); and (ii) to evaluate the relationship between the derived data and determine their relative influence on the lagoon environment. The derived data were subjected to descriptive statistics, and relationships were explored using Pearson's correlation and regression analysis. The effect of land cover on LST was measured using the Contribution Index and a trend analysis was carried out. From the results, the mean LSTs for the four years were 22.68°C (1984), 24.34°C (2002), 26.46°C (2013) and 28.40°C (2019). Generally, the mean LSTs is in opposite trend with the mean NDVIs and EVIs as associated with their dominant land cover type. The strongest positive correlations were observed between NDVI and EVI while NDVI had the closest fit with LST in the regression. Built-up areas have the highest contributions to LST while vegetation had a cooling influence. The depletion in vegetative cover has compromised the biodiversity of this environment and efforts are required to reverse this trend.

KEY WORDS: Coastal Environment, Remote Sensing, Land Cover, LST, NDVI, EVI, Lagos Lagoon

Corresponding author: Chukwuma J. Okolie, cokolie@unilag.edu.ng

Introduction

Lagoons are located on the coastal shore and are environmentally resourceful as a result of their biodiversity (Panda, Mohanty 2008). For example, the lagoon wetlands, wherever they exist, are useful for their numerous economic contributions to coastal dynamic balance and biological diversity. Also, they support numerous natural services and functions freely delivered by the ecosystem and human habitats which are highly

valued by society. These services or functions include sediments and nutrient retention, storm protection, food and storage distribution, and improvement of water quality (Kindscher et al. 1998, Obiefuna et al. 2013a). Degradation in the lagoon environment could certainly lead to a reduction or total loss of all these services and functions. Coastal lagoon environments, especially across the developing countries, are under increased pressure by human population growth, changing lifestyles, growing demands for natural

resources and socio-economic factors (Panigrahi et al. 2007, Kolios, Stylios 2013). It has become a trend in a geometrical progression that population increases along with rural or urban activities around coastal lagoons. The intensity of these activities and the impacts are directly proportional to urban growth. It is interesting to know that the lagoon and its ecosystem features result in high changeability in short Spatio-temporal scales of the surrounding communities. At a comparatively low cost and faster rate, remote sensing appears to be the most applied mechanism for detecting Spatio-temporal transformations and assessing the trend of land cover changes in the coastal environments using multi-temporal analysis (Green et al. 1996). Remote sensing provides a resolution that is indispensable for the sustainable management of the landscape of coastal ecosystems to mitigate irreparable degradation caused by anthropogenic activities as a result of the misuse of natural resources (Adegun et al. 2015, Ajibola et al. 2012, 2016).

The intensity of anthropogenic activities and urban development worldwide are related to changes in land cover and vegetation and have disrupted the balance of natural ecosystems (Ngie et al. 2016, Meera et al. 2015, Mushtaq, Asima 2016). Land cover, Land Surface Temperature (LST) and Vegetation Indices (VIs) are regarded as significant parameters for monitoring environmental changes. According to Qiu et al. (2018), LST is an important variable in climate and environmental research. The traditional method for estimating LST is by direct measurement using instruments set-up at meteorological stations. The limitation of this approach is the inability to map LST over large-scale areas and this is where satellite remote sensing presents several advantages. For decades, the use of satellite-derived data for estimating LST has been well reported in the literature (Jimenez-Munoz, Sobrino 2003, Zhang et al. 2006, Xiao et al. 2007, David 2008, Nwilo et al. 2012, Oguz 2013, Zaharaddeen et al. 2016, Jeevalakshmi et al. 2017, Deng et al. 2018, Tarawally et al. 2018). It has also been suggested that the inclusion of LST can improve land cover and vegetation monitoring (Mildrexler et al. 2007, 2009, Sobrino, Julien 2013, Phompila et al. 2015). Also, change in land cover is an important indicator that affects LST. Because the surface reflectance and topography of land cover types

are different, it also leads to differences in LST (Hou et al. 2010). Moreover, in the context of urbanisation, Li et al. (2017) discovered that an increase in anthropogenic activities is the main factor that enhances the rapid change of land cover. Consequently, it is expedient that the relationship between LST and land cover should be monitored, especially in coastal regions where urban expansion is on the increase. Rapid urban expansion, especially in coastal regions, has caused land cover changes. This affects environmental processes at local and regional levels, especially the urban heat island (UHI) (Streutker 2003, Weng 2003). The urban thermal environment is mainly controlled by the distribution of LST, which is a direct result of the increase in urbanisation (Sun et al. 2011).

Understanding environmental changes also require effective monitoring of VIs. VIs are arithmetic combinations of two or more bands related to the spectral characteristics of vegetation (Matsushita et al. 2007) and have found wide applications in crop phenology monitoring, vegetation classification and derivation of vegetation biophysical parameters. Generally, VI values are in the range from -1 to $+1$. Negative VI values indicate the presence of cloud, snow, water or urban land whereas positive VI values are positively correlated with green vegetation (Chen et al. 2006a). According to Phompila et al. (2015), the majority of remote sensing techniques for monitoring vegetation cover changes have utilised VIs, most commonly the Normalised Difference Vegetation Index (NDVI) and the Enhanced Vegetation Index (EVI). Of these two, the NDVI is the most commonly used. When applied to vegetation monitoring, it can cancel out a large proportion of the noise caused by topographic effects, clouds or cloud shadow, changing sun angles and atmospheric conditions (Huete, Justice 1999, Matsushita et al. 2007). It has found wide applications because it is accurate, computationally simple, efficient and useful for agricultural land use mapping in tropical environments (Meera et al. 2015). However, it is more saturated at high biomass levels (Gao et al. 2000) and also sensitive to canopy background variations (Huete 1988). As an enhancement to the NDVI, the EVI improves on atmospheric correction, index saturation in densely forested areas and reduction of soil reflectance influence

(Boegh et al. 2002, Huete et al. 2002, Gao et al. 2003, Xiao et al. 2004, Rankine et al. 2017). The EVI also provides a more dynamic range than the NDVI, and its improved performance has brought it to the attention of many researchers. Li et al. (2010) assessed the correlation of NDVI and EVI derived from the Moderate Resolution Imaging Spectroradiometer (MODIS) instrument with natural vegetation coverage in the Northern Hebei Province of China. Their study showed that MODIS-NDVI was more correlated with field data of vegetation cover and had obvious advantages for predicting natural vegetation coverage than MODIS-EVI. Therefore, there still exists a need to combine the complementary performances of NDVI and EVI for a detailed understanding of vegetation characteristics and inform planning decisions for more sustainable environments.

Furthermore, VIs are another factor that influences changes in LST by selectively reflecting and absorbing radiation energy from the sun and modifying latent and functional heat exchange (Yuan et al. 2017). Vegetation abundance reduces LSTs through latent heat transfer from the surface to atmosphere via the process of evapotranspiration (Farina 2012). As such, NDVI and EVI can be exploited to assess this relationship thereby providing useful insights into the natural cooling mechanism of vegetation. It has also been shown that land cover characteristics have a significant influence on environmental thermal conditions in the environment (Xian, Crane 2006, Roth 2008). Also, LST is influenced by land cover change and this is due to its role in the exchange of energy on the earth's surface, surface matter exchange and atmospheric processes (both physical and chemical) (Xiao et al. 2007, Butuc, Moldovean 2011, Deng et al. 2018). In a recent study, Ferrelli et al. (2018) observed LST variation within diverse land covers in Monte Hermoso City, Argentina, as a consequence of urban growth and changes in vegetation cover. They thereafter concluded that the Spatio-temporal variation of LST values may indicate modifications in urban land cover. The effect of population growth and the pressure or degradation it exerts on the environment are also other motivations to explore the relationship between land cover change and LST variations (Kaufmann et al. 2007, Ferrelli et al. 2018).

Remote sensing techniques permit the development of high resolution temporal and spatial results (Ferrelli et al. 2018). In recent times, researchers have studied and documented the changes in the coastal environments of Nigeria with remote sensing methods. Such studies include observations of changes in the Lower Ogun River flood plain (Odunuga, Oyebande 2007), evaluation of the degree of mangrove ecosystem changes in the Niger Delta (James et al. 2007), application of satellite remote sensing in monitoring land degradation along the coast of Ondo in Nigeria (Abbas 2008, Abbas, Fasona 2012), wetland changes in the Lagos/Lekki lagoon environments (Obiefuna et al. 2013a, 2013b) and dynamics of land cover and LST changes in Lagos metropolis (Obiefuna et al. 2018). However, the link between land cover, LST and VIs has not been well exploited in the monitoring of the Lagos Lagoon environment. Therefore, the objectives of this study are to: (i) estimate through satellite imagery analysis the extent of changes in the Lagos Lagoon environment from 1984 to 2019 using the derived data on land cover, LST, NDVI and EVI and (ii) evaluate the relationship between the derived data and determine their relative influence on the lagoon environment.

Study Area

The study area is a region encompassed by a portion of the local government areas (LGAs) surrounding the Lagos Lagoon in Lagos State, south-western Nigeria. The Lagos Lagoon is a part of the continuous system of lagoons and creeks that are found in the Barrier-Lagoon complex along the coast of Nigeria in West Africa. The geographic extent of the lagoon is between longitudes 3°21'00"-3°57'50"E and latitudes 6°23'30"-6°41'10"N. The lagoon receives its discharge from River Ogun and River Osun and the system empties into the Atlantic Ocean via the Lagos harbour. Lagos State is located within the tropical rain forest belt, and the dominant vegetation is the tropical swamp forest which consists of fresh water and mangrove swamp forests (Ojeh et al. 2016). Due to the interaction between the warm, humid maritime tropical air mass and the hot and dry continental air mass from the interior parts of Nigeria, the state experiences

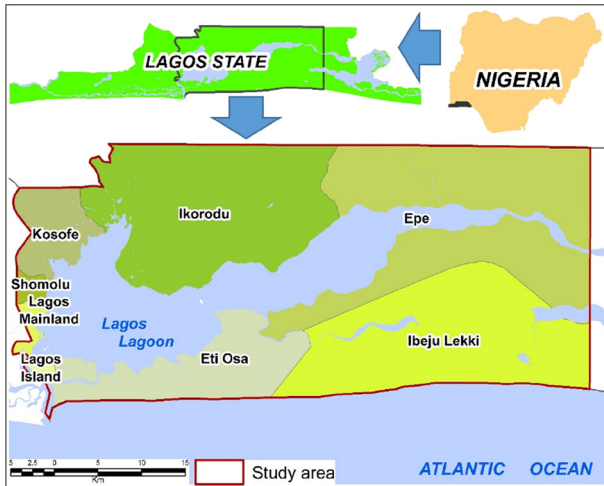


Fig. 1. Map showing the study area.

two seasons: a rainy or wet season from April to October and a dry season from November to March (Fasona et al. 2005, Ojeh et al. 2016, Nwilo et al. 2020). These seasons are under the influence of the intertropical convergence zone (ITCZ) that moves along with the position of highest rainfall (Salau et al. 2016, Akpootu et al. 2017). While the wet season is characterised by heavy rainfall, the dry season is characterised by little or no rainfall with a dry dust-laden atmosphere (Akpootu et al. 2017). However, some areas in Lagos State that are very close to the Atlantic Ocean experience rainfall throughout the year (Aribisala et al. 2016, Akpootu et al. 2017). Humidity is very high throughout the year and monthly average maximum temperatures range from 28.6°C (July/August) to 33.7°C (February/March) (Ojeh et al. 2016). Figure 1 presents a map showing the location of the study area.

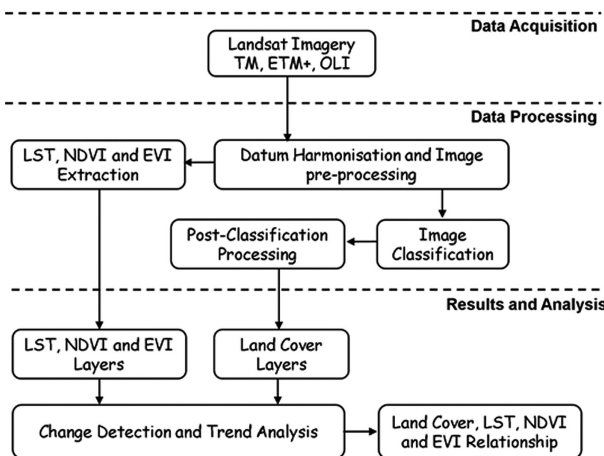


Fig. 2. The workflow of the methodology.

Materials and methods

The methodology workflow is shown in Figure 2.

Data Acquisition, Harmonisation and Pre-processing

Medium resolution Landsat imageries for 4 years were acquired from the United States Geological Surveys Earth Explorer portal (USGS 2020). On the Earth Explorer webpage, the appropriate search criteria were set and the image-ries were downloaded. Following the approach of Ferrelli et al. (2018), imageries with excessive cloud cover were discarded. To maximise the coverage of the available scenes, a combination of Landsat scenes (191/055 and 191/056) was done to form a complete coverage of the study area at four average periods: 1984 (Thematic Mapper (TM)), 2002 (Enhanced Thematic Mapper (ETM+)), 2013 and 2019 (Operational Land Imager (OLI)/Thermal Infrared Sensor (TIRS)). These imageries are already geometrically corrected by USGS and ortho-rectified to Level 1 (Tatem et al. 2006, Gutman et al. 2013). A further confirmation of the geometric/positional suitability of the Landsat scenes was done with reference to the Lagos State boundary along the Lagos shoreline through overlay and the alignment was satisfactory. The scenes used for land cover classification covered the following periods: TM (1984–1986), ETM+ (2001/2002) and OLI (December 2013 and January 2019); while scenes used for LST determination covered the following: TM (December 1984), ETM+ (February 2000) and TIRS (December 2013 and January 2018). For NDVI and EVI extraction, the image-ry dates are as follows: TM (December 1984), ETM+ (December 2002) and OLI (December 2013 and January 2019). Generally, the imageries cover dry season months. The Landsat imageries have a pixel spacing of 30 m and are referenced to a Universal Transverse Mercator (UTM) co-ordinate system defined on the WGS84 datum (WGS84 UTM Zone 31N).

Image Classification

Following the approach of Ullah et al. (2019), the first step involved a preliminary

Table 1. Description of the land cover categories used in the study.

Land cover class	Description
Built-up area	This feature class encompasses settlements within the study area
Bare land	Paved surfaces, exposed topsoil
Water body	This encompasses all surface water bodies visible on the imagery
Vegetation	Shrubs, grasslands, cultivated lands, wetlands and mangroves

interpretation of the Landsat imageries aided by Anderson's (1971) Level I Classification Scheme and the use of Google Earth imagery for training sites development. This interpretation categorised the study area land cover into four classes, such as bare land, built-up area, vegetation and water body (Table 1). Next, training sites were created for each class and the imageries were then subjected to supervised classification by the Maximum Likelihood Classifier (MLC) in ENVI 5.3 image processing software. MLC incorporates the variance-covariance within the class distributions and for data that has a normal distribution; it gives a better performance than other known parametric classifiers. It performs well over various types of land cover, satellite systems and conditions (Bolstad, Lillesand 1991). It is a preferred choice for many applications and its good performance has been proven (Sharma et al. 2017, Brendel et al. 2019). After classification, the feature classes were transferred to ArcGIS for editing, refinement and assessment of classification accuracy. According to Hasmadi et al. (2009), accuracy assessment is important for checking the reliability of the classification results. The main idea behind any image classification process is to obtain the highest accuracy possible (Sharma et al. 2011). The minimum level of interpretation accuracy in the identification of land cover classes from remotely sensed data should be at least 85% (Anderson 1971). Using the Landsat imagery as a reference, 90 points were used to compare features interpreted on the imageries and their corresponding output in the classification. The point comparison detected the correctly classified pixels, pixels assigned to a certain class that did not belong to it (commission errors) and pixels that belong to one class but are included into other classes (omission errors) (Tran et al. 2017, Aboelnour, Engel 2018). The overall accuracy was then computed using the following expression:

$$\text{Overall accuracy (\%)} = \frac{\text{Total number of correct samples}}{\text{Total number of samples}} \times 100 \quad (1)$$

NDVI and EVI Determinations

Traditionally, the NDVI is calculated using a combined operation between the Red band and Near-Infrared (NIR) band (Qiu et al. 2018, Ferrelli et al. 2018, Ullah et al. 2019, Guha et al. 2020) as follows:

$$\text{NDVI} = (R_{\text{NIR}} - R_{\text{Red}}) / (R_{\text{NIR}} + R_{\text{Red}}) \quad (2)$$

where:

- R_{NIR} represents the spectral reflectance in the NIR band,
- R_{Red} represents the spectral reflectance of the Red band.

The EVI is computed (Hoek van Dijke et al. 2019, Semeraro et al. 2020) as follows:

$$\text{EVI} = G \times ((R_{\text{NIR}} - R_{\text{Red}}) / (R_{\text{NIR}} + C_1 \times R_{\text{Red}} - C_2 \times R_{\text{Blue}} + L)) \quad (3)$$

where:

- G is the Gain factor,
- R_{NIR} , R_{Red} and R_{Blue} are atmospherically corrected/partially atmosphere-corrected (Rayleigh and ozone absorption) surface reflectance,
- L is the canopy background adjustment to address non-linear, differential NIR and red radiant transfer through a canopy,
- C_1 and C_2 are coefficients of the aerosol resistance term, which uses the Blue band to correct for aerosol influences in the Red band.

These enhancements incorporated into EVI reduce the background noise, atmospheric noise and saturation in most cases.

Landsat Level 2 NDVI and EVI products were ordered and downloaded from the USGS Earth Resources Observation and Science (EROS) Centre Earth Science Processing Architecture on-demand interface. The ESPA is an incubation environment that provides users with an on-demand interface to process and customise Landsat science products (USGS 2020). The coefficients adopted on ESPA in the EVI algorithm for Landsat 4-7 and Landsat 8 are $G = 2.5$, $C_1 = 6$, $C_2 = 7.5$ and $L = 1$. The Level 1 scene lists were uploaded on the interface and processing was

done for the surface reflectance, NDVI and EVI Level 2 products. The surface reflectance enhances comparison between multiple Landsat imageries over the study area by considering atmospheric effects such as aerosol scattering and thin clouds, which can help in the detection and characterisation of surface changes. According to USGS (2019), *surface reflectance is generated from Level-1 inputs that meet the <76° solar zenith angle constraint and include the required auxiliary data inputs to generate a scientifically viable product.* The NDVI and EVI products were delivered from ESPA as single bands with 16-bit integers and values ranging from -10,000 to +10,000 (USGS 2020). However, using the given scale factor of 0.0001, this was scaled down to a range from -1 to +1.

LST Retrieval

The retrieval of LST followed the single-channel method (Oguz 2013, Ferrelli et al. 2015, Obiefuna et al. 2018). Landsat TM thermal Band 6, ETM Band 6_1 and TIRS Band 10 were used for the retrieval. The key stages of the methodology are discussed below.

Conversion of digital number (DN) to spectral radiance

The formula for converting DN in Landsat 5 and 7 to spectral radiance is given by Zareie et al. (2016):

$$L_{\lambda} = \left(\frac{LMAX - LMIN}{QCALMAX - QCALMIN} \right) \times (QCAL - QCALMIN) + LMIN \quad (4)$$

where:

- L_{λ} is spectral radiance at the sensor's aperture ($W m^{-2} sr^{-1} \mu m^{-1}$),
- QCAL is quantized calibrated pixel value in DN,
- LMIN is spectral radiance scaled to QCALMIN,
- LMAX is spectral radiance scaled to QCALMAX,
- QCALMIN is minimum quantized calibrated pixel value (corresponding to LMIN) in DN,
- QCALMAX is maximum quantized calibrated pixel value (corresponding to LMAX) in DN.

The formula to derive the spectral radiance for Landsat 8 is given by USGS (2015):

$$L_{\lambda} = M_L \times QCAL + A_L \quad (5)$$

where:

- M_L is Radiance multiplicative scaling factor for the band,
- A_L is Radiance additive scaling factor for the band.

The values for LMIN, LMAX, QCALMIN, QCALMAX, M_L and A_L are derived from the Landsat metadata file.

Conversion of spectral radiance to top-of-atmosphere (TOA) brightness temperature

After calculating the spectral radiance (L_{λ}), the next step was the calculation of the TOA brightness temperature. The TOA approximation formula is given by Dewan and Corner (2012), Zareie et al. (2016), Hamoodi et al. (2019) and Guha et al. (2020):

$$T = K_2 / \log(1 + K_1 / L_{\lambda}) \quad (6)$$

where:

- T is TOA brightness temperature (K),
- K_1 ($W cm^{-2} sr^{-1} \mu m^{-1}$) and K_2 (K) are pre-launch calibration constants.

Values for K_1 and K_2 for Landsat TM and ETM+ are shown in Table 2, whereas Table 3 shows the values for Landsat 8 TIRS.

Table 2. Landsat TM and ETM+ Thermal Band Calibration Constants.

	Landsat 5 TM	Landsat 7 ETM+
K_1	607.76	666.09
K_2	1260.56	1282.71

Table 3. Landsat 8 TIRS Thermal Band Calibration Constants.

	Band 10	Band 11
K_1	774.89	480.89
K_2	1321.08	1201.14

Conversion of brightness temperature to LST

The brightness temperature was subsequently converted to LST using Eq. (7) (Hamoodi et al. 2019, Ullah et al. 2019):

$$S_T = \frac{T}{1 + (\lambda \times T / \rho) \log \epsilon} \quad (7)$$

where:

- S_T is LST (K),

- λ is Wavelength of emitted radiance (11.5 μm),
- ε is Land surface emissivity (typically 0.95),
- $\rho = h \times c / \sigma = 1.438 \times 10^{-2} \text{ m K}$ (σ = Boltzmann constant = $1.38 \times 10^{-23} \text{ J K}^{-1}$, h = Planck's constant = $6.626 \times 10^{-34} \text{ J s}$, c = velocity of light = $2.998 \times 10^8 \text{ m s}^{-1}$).

Finally, the LST in Kelvin was converted to degree Celsius by subtracting from 273.15.

Relationships, Change Detection and Trend Analysis

Statistical analyses are commonly applied to establish relationships between parameters, for example, Land cover-LST (Dewan, Corner 2012), LST-NDVI (Ferrelli et al. 2018, Hamoodi et al. 2019, Malik et al. 2019, Ullah et al. 2019, Guha et al. 2020, Mukherjee, Singh 2020), NDVI-EVI (Chen et al. 2006b, Matsushita et al. 2007, Li et al. 2010, Uyeda et al. 2017) and LST-EVI (Phompila et al. 2015). In this study, an inventory of the parameters was created for the study area. To do this, the LST, NDVI and EVI raster maps were converted to grids of point shape files with the associated parameter values at pixel centres in the attribute table. The grids were then overlaid on the land cover, LST and NDVI maps within ArcGIS. The values on the land cover maps coinciding with the points were extracted. To explore the relationship between the parameters, descriptive statistics were computed using the Statistical Package for the Social Sciences (SPSS) software v20. In line with Guha et al. (2020), the minimum, maximum, mean and standard deviations (SDs) of the parameters were generated. Pearson's correlation analysis was used to analyse the correlation between variables. Linear regression was also carried out to determine the temporal relationship between the LST, NDVI and EVI in different land cover classes. The effect of land cover on the LST was calculated using the Contribution Index (CI). The CI quantifies the warming or cooling extent of a land cover type and this is related to the proportion of the total land area it occupies. It links spatial structure and long-term changes in land cover to LST intensities. The equation for calculating the CI is given by Eq. (8) (Odindi et al. 2015, Odindi et al. 2017, Tarawally et al. 2018).

$$CI = D_i \times S \quad (8)$$

where:

- D_i is the average LST of study area minus average LST of land cover class type,
- S is the ratio of area covered by land cover type to the total area of the study area.

If CI of a land cover type is positive, it indicates that it contributes to raising the LST and vice versa.

Going further, a trend analysis was carried out using the Mann-Kendall test and Sen's estimator of slope. The Mann-Kendall's test is a non-parametric test for trend analysis (Gilbert 1987). It is particularly useful as the data need not conform to any particular distribution (Hamed 2008). The use of mean values of multiple observations in a period was recommended by Gilbert (1987) for Mann-Kendall trend analysis. If the Mann-Kendall's statistic (S) is a large positive number, measurements taken later in time tend to be larger than those taken earlier. Similarly, if S is a large negative number, measurements taken later in time tend to be smaller. The first scenario is to test the null hypothesis (H_0) of no trend against the alternative hypothesis (H_A) of an upward trend. H_0 is rejected in favour of H_A if S is positive and if the probability value is less than the significance level (p -value) of the test. Similarly, to test H_0 against the alternative hypothesis H_A of a downward trend, H_0 is rejected and H_A accepted if S is negative and if the probability value is less than the a priori specified p -value. For this study, a trend analysis of the LST, NDVI and EVI was done for the years 1984, 2002, 2013 and 2019. The Sen's slope estimator, Q_{med} (Sen 1968, Gocic, Trajkovic 2013), is the magnitude of the upward trend per year. The variables with the upward trend or linear trend were further probed for the annual increase or slope value. The Q_{med} sign reflects data trend reflection, while its value indicates the steepness of the trend.

Results and discussion

Analysis of Land Cover Changes

Table 4 shows the areal distribution of land cover in the study area for the years 1984, 2002, 2013 and 2019. The analysis shows that bare land increased by 613.7% from 7.08 km^2 in 1984

Table 4. Areal distribution of land cover in 1984, 2002, 2013 and 2019.

S/N	Land cover class	1984		2002		2013		2019	
		km ²	%						
1	Bare land	7.08	0.40	50.53	2.83	13.65	0.76	24.85	1.39
2	Built-up area	40.77	2.28	130.34	7.30	416.27	23.32	441.49	24.73
3	Vegetation	1321.78	74.05	1199.50	67.20	956.68	53.60	933.83	52.32
4	Water body	415.37	23.27	404.63	22.67	398.40	22.32	384.83	21.56
	Total	1785.00	100.00	1785.00	100.00	1785.00	100.00	1785.00	100.00

to 50.53 km² in 2002 (at the rate of 2.41 km² a⁻¹). Thereafter, it decreased by 72.99% to 13.65 km² between 2002 and 2013 (at the rate of 3.35 km² a⁻¹) and finally decreased by 82.05% to 24.85 km² between 2013 and 2019 (at the rate of 1.87 km² a⁻¹). Built-up areas that occupied only 40.77 km² in 1984 expanded significantly by 219.7% to 130.34 km² between 1984 and 2002 (at the rate of 4.98 km² a⁻¹) and subsequently increased by 219.37% to 416.27 km² between 2002 and 2013 (at the rate of 25.99 km² a⁻¹). Between 2013 and 2019, it increased slightly by 6.06% to 441.49 km² (at the rate of 4.20 km² a⁻¹). There were depletions in the coverage of vegetation within the area. Between 1984 and 2002, 9.25% of the vegetation cover (122.28 km²) was lost at the rate of 6.79 km² a⁻¹. In the period between 2002 and 2013, 20.24% of vegetation cover representing 242.82 km² was lost at the rate of 22.07 km² a⁻¹. Finally, 2.39% of vegetation cover (22.85 km²) was lost between 2013 and 2019 (at the rate of 3.81 km² a⁻¹). In relation to other land cover classes, the loss in water body was moderate over the entire period. Water body decreased from 415.37 km² in 1984 to 404.63 km² in 2002, 398.40 km² in 2013 and finally dropped to 384.83 km² in 2019.

The accuracy assessment of the classification yielded the following overall accuracies: 96.67% (1984), 81.11% (2002), 93.33% (2013) and 87.78% (2019).

Land Cover, LST, NDVI and EVI Distributions

Tables 5–8 show descriptive statistics of the LST, NDVI and EVI per land cover excluding water body for the years 1984, 2002, 2013 and 2019, respectively. The mean LSTs for the four periods are 22.68°C (1984), 24.34°C (2002), 26.46°C (2013) and 28.40°C (2019), respectively. Comparison was done with historical monthly temperatures of Lagos from WWO (2020). The online temperature data showed that the state had average temperatures of 28°C in both December 2013 and January 2018. These monthly averages are in the same range of the average LSTs from Landsat shown in Tables 7 and 8. The trend reveals a gradual rise in surface temperatures and warmth within the environment surrounding the Lagos Lagoon over the years. The lowest temperature recorded was 17.63°C in 1984 whereas the highest temperature was 36.90°C in 2019.

Table 5. Descriptive statistics of the LST, NDVI and EVI relationship with land cover in 1984.

Parameter	Land cover class	N	Mean	SD	95% Confidence Interval for Mean		Min	Max
					Lower Bound	Upper Bound		
LST [°C]	Bare land	859	25.31	1.04	25.24	25.38	21.30	27.93
	Built-up area	5036	26.39	0.80	26.36	26.41	22.67	29.18
	Vegetation	161051	22.55	1.10	22.54	22.55	17.63	29.14
	Total	166946	22.68	1.29	22.67	22.68	17.63	29.18
NDVI [-]	Bare land	859	0.13	0.04	0.13	0.13	0.05	0.33
	Built-up area	5036	0.14	0.04	0.14	0.14	0.01	0.28
	Vegetation	161051	0.38	0.06	0.38	0.38	0.00	0.50
	Total	166946	0.37	0.07	0.37	0.37	0.00	0.50
EVI [-]	Bare land	859	0.10	0.03	0.10	0.10	0.03	0.26
	Built-up area	5036	0.10	0.03	0.10	0.10	0.01	0.20
	Vegetation	161051	0.27	0.05	0.27	0.27	0.00	0.41
	Total	166946	0.27	0.06	0.27	0.27	0.00	0.41

The built-up area class had the highest mean LST values while vegetation had the lowest mean values. The NDVI values ranged from 0.0 to 0.5 (1984), -0.2 to 0.70 (2002), -0.12 to 0.85 (2013) and -0.06 to 0.80 (2019). For the EVI, the ranges are as follows: from 0.0 to 0.41 (1984), -0.08 to 0.56 (2002), -0.05 to 0.74 (2013) and -0.04 to 0.60 (2019). In Lagos State, many patches of bare land are sandwiched between built-up areas. Hence, this mixed set-up could explain the little differentiated values between the NDVIs of bare land and built-up area. It has been discovered

Table 6. Descriptive statistics of the LST, NDVI and EVI relationship with land cover in 2002.

Parameter	Land cover class	N	Mean	SD	95% Confidence Interval for Mean		Min	Max
					Lower Bound	Upper Bound		
LST [°C]	Bare land	5948	26.06	1.04	26.03	26.08	22.74	29.85
	Built-up area	15698	26.25	0.99	26.24	26.27	22.95	29.55
	Vegetation	145300	24.06	0.95	24.06	24.07	22.36	29.64
	Total	166946	24.34	1.20	24.33	24.35	22.36	29.85
NDVI [-]	Bare land	5948	0.25	0.09	0.25	0.26	0.01	0.52
	Built-up area	15698	0.26	0.12	0.26	0.27	0.00	0.59
	Vegetation	145300	0.56	0.08	0.56	0.56	-0.20	0.70
	Total	166946	0.52	0.13	0.52	0.52	-0.20	0.70
EVI [-]	Bare land	5948	0.16	0.05	0.16	0.16	0.01	0.35
	Built-up area	15698	0.16	0.08	0.16	0.16	0.00	0.42
	Vegetation	145300	0.35	0.06	0.35	0.35	-0.08	0.56
	Total	166946	0.32	0.09	0.32	0.32	-0.08	0.56

Table 7. Descriptive statistics of the LST, NDVI and EVI relationship with land cover in 2013.

Parameter	Land cover class	N	Mean	SD	95% Confidence Interval for Mean		Min	Max
					Lower Bound	Upper Bound		
LST [°C]	Bare land	1460	28.80	1.82	28.70	28.89	24.46	34.15
	Built-up area	49568	29.34	1.90	29.32	29.35	23.80	36.31
	Vegetation	115918	25.20	1.31	25.19	25.21	23.09	34.73
	Total	166946	26.46	2.43	26.45	26.47	23.09	36.31
NDVI [-]	Bare land	1460	0.25	0.12	0.24	0.26	0.05	0.63
	Built-up area	49568	0.37	0.13	0.37	0.38	-0.12	0.72
	Vegetation	115918	0.70	0.09	0.70	0.70	-0.12	0.85
	Total	166946	0.60	0.18	0.60	0.60	-0.12	0.85
EVI [-]	Bare land	1460	0.18	0.08	0.18	0.19	0.04	0.43
	Built-up area	49568	0.23	0.09	0.23	0.23	-0.04	0.53
	Vegetation	115918	0.43	0.07	0.43	0.43	-0.05	0.74
	Total	166946	0.37	0.12	0.37	0.37	-0.05	0.74

Table 8. Descriptive statistics of the LST, NDVI and EVI relationship with land cover in 2019.

Parameter	Land cover class	N	Mean	SD	95% Confidence Interval for Mean		Min	Max
					Lower Bound	Upper Bound		
LST [°C]	Bare land	2598	29.17	1.30	29.12	29.22	23.17	32.45
	Built-up area	52944	29.80	1.46	29.79	29.82	19.48	34.81
	Vegetation	111404	27.72	1.36	27.71	27.73	20.51	36.90
	Total	166946	28.40	1.70	28.40	28.41	19.48	36.90
NDVI [-]	Bare land	2598	0.29	0.12	0.29	0.30	0.01	0.68
	Built-up area	52944	0.27	0.10	0.27	0.28	-0.02	0.68
	Vegetation	111404	0.56	0.11	0.56	0.56	-0.06	0.80
	Total	166946	0.47	0.17	0.47	0.47	-0.06	0.80
EVI [-]	Bare land	2598	0.19	0.07	0.19	0.20	0.01	0.43
	Built-up area	52944	0.16	0.06	0.16	0.16	-0.01	0.48
	Vegetation	111404	0.34	0.07	0.34	0.34	-0.04	0.60
	Total	166946	0.28	0.11	0.28	0.28	-0.04	0.60

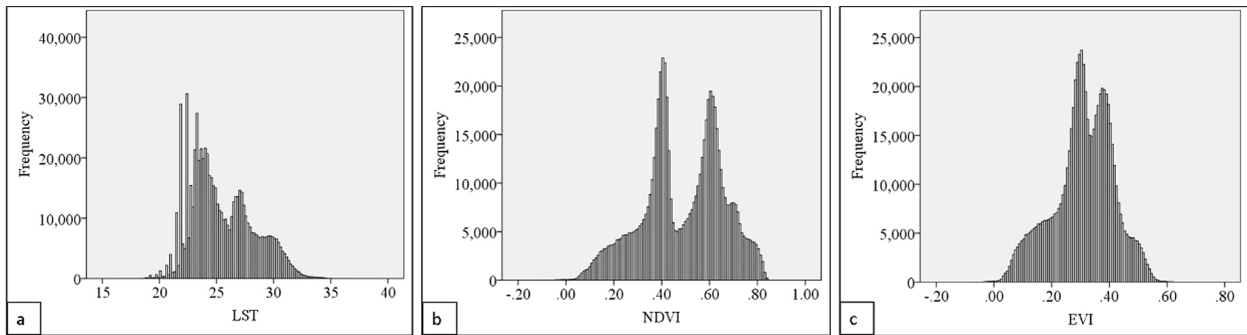


Fig. 3. Histograms showing a range of values from 1984 to 2019 for LST (a), NDVI (b), and EVI (c).

that the values of EVI are generally lower than the NDVI values. This is due to the atmospheric correction and reduction of soil reflectance influence, which has been factored in the EVI model. Figure 3 is the histogram representation of the range of values of LST, NDVI and EVI, respectively, from 1984 to 2019. The histogram shows the dominance of LST values within the range of 23–24°C, the NDVI values within the ranges, 0.35–0.42 and 0.58–0.62 dominate the Lagos Lagoon environment over the years, the EVI values within the range of 0.30–0.40 dominate the Lagos Lagoon environment over the years. These values of VI show the dominance of greenness in the Lagos Lagoon environment despite the urbanisation. Figures 4–7 present maps of land cover, LST, NDVI and EVI for the periods under study. The progressive increase in built-up areas and the decrease in vegetation cover are evident in Figure 4. The LST map also shows a progressive rise in temperatures emanating from the centre of the metropolis. Juxtaposing the four maps, it can be deduced that the lagoon environment has varied vegetation where vegetation decline over the 35 years follows a pattern of increasing disappearance from the west to the east. This also indicates that urban development is very high in the west and it increases yearly towards the north-western and eastern regions of the lagoon environment. Generally, the vegetation-covered areas have the highest NDVI and EVI values. Areas with abundant vegetation cover display low LST values (Guha et al. 2020). The trend of overall LST ranging from higher to lower for built-up areas, bare land and vegetation conforms with the findings of Ullah et al. (2019).

Analysis of Relationship between Parameters

Figures 8–10 present graphical illustrations of the mean LSTs, NDVIs and EVIs associated with land cover types in the eight LGAs surrounding the Lagos Lagoon with error bars representing ± 1 SD. The eight LGAs (Lagos Island, Somolu, Ibeju Lekki, Ikorodu, Somolu, Epe, Eti-Osa and Kosofe) with their spatial locations show varying degrees of urbanisation. The highest mean LST values are observed in Lagos Island, Lagos Mainland and Somolu LGAs and this is possible because of the high population growth rate and urbanisation, which invariably causes a high degree of human-induced heat. Hence, the increase in urbanisation must have resulted to high mean values of LST in each of the years of study. This is one of the effects of UHI. Notwithstanding, areas such as the extreme eastern part of Ikorodu, Ibeju-Lekki and Epe exhibit the highest means of NDVI and EVI values (Figs 9 and 10). This might be attributed to the predominance of vegetation cover. In agreement with the findings of Wilson et al. (2003) and Yue et al. (2007), green vegetation cover in the areas suggests relatively a higher rates of evapotranspiration and favouring of latent exchange between surface and atmosphere as compared with built-up areas. In the study by Ferrelli et al. (2018) on the Spatio-temporal relationship between LST and NDVI in Monte Hermoso City, Argentina, minimum NDVI was observed in summer whereas the LST showed the opposite behaviour. Similarly, in the present study which was conducted with Landsat images acquired in the dry season, it is observed that mean LSTs are in opposite trend with the mean

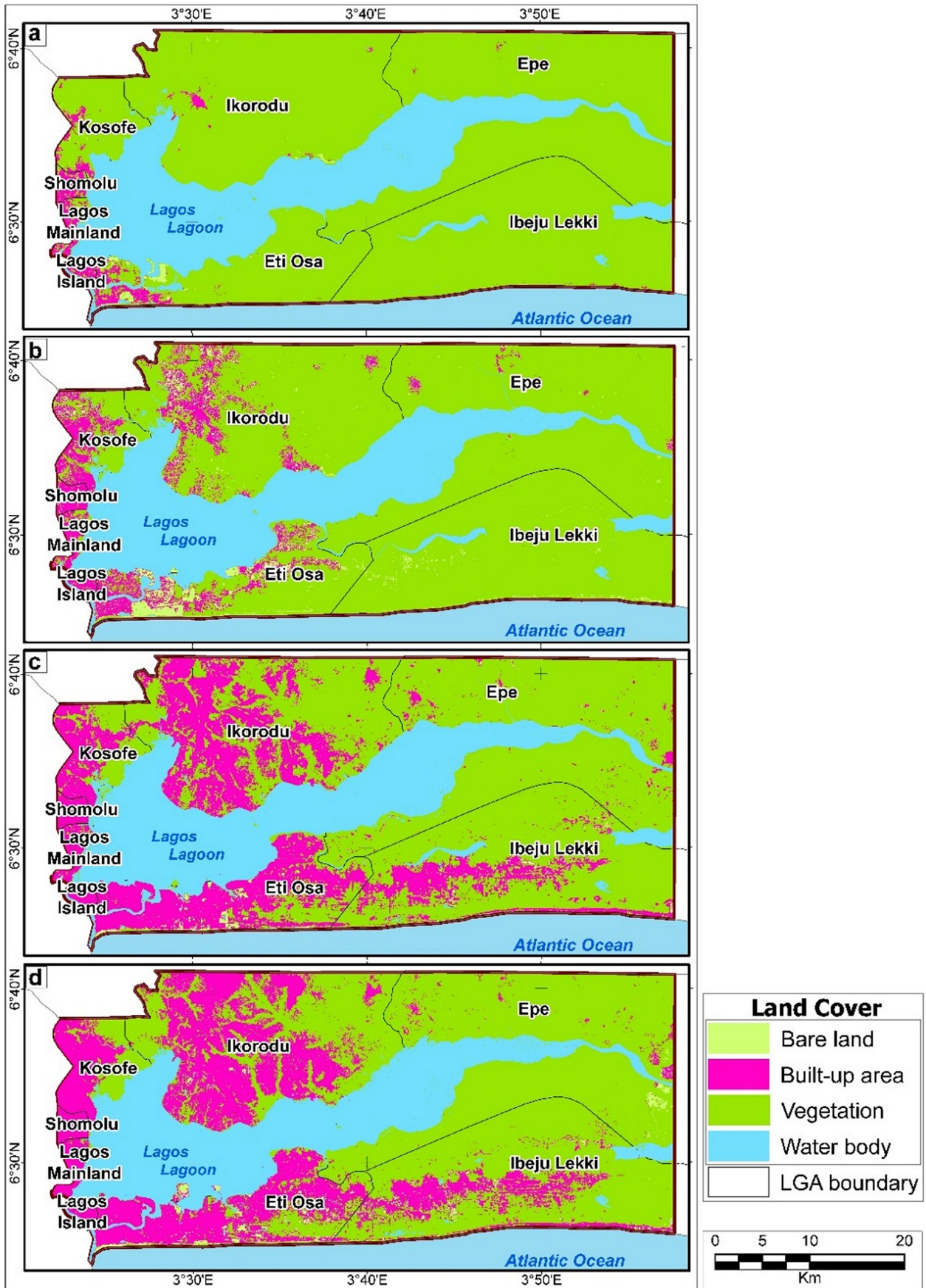


Fig. 4. Spatial pattern of land cover for 1984 (a), 2002 (b), 2013 (c) and 2019 (d).

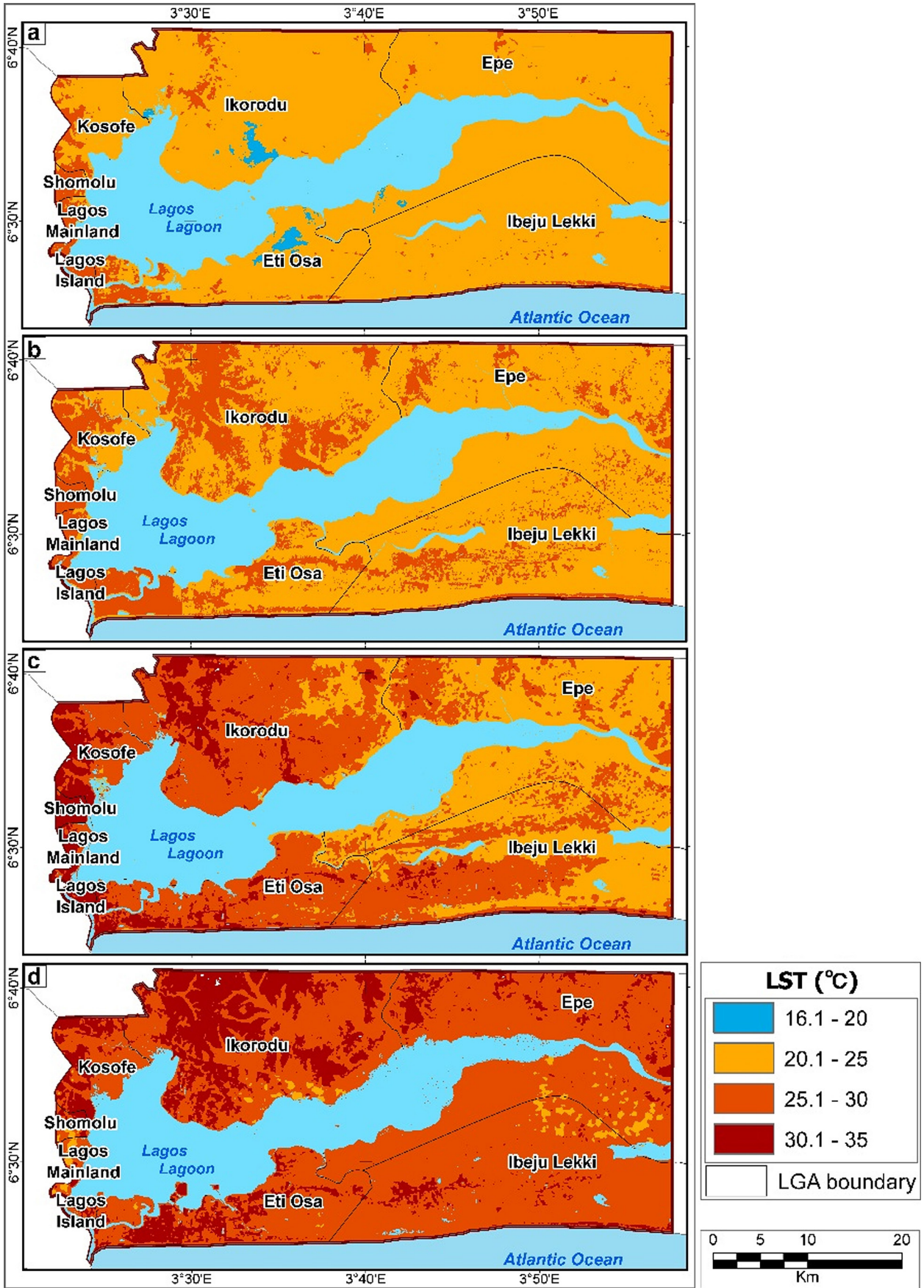


Fig. 5. Spatial pattern of LST for 1984 (a), 2002 (b), 2013 (c) and 2019 (d).

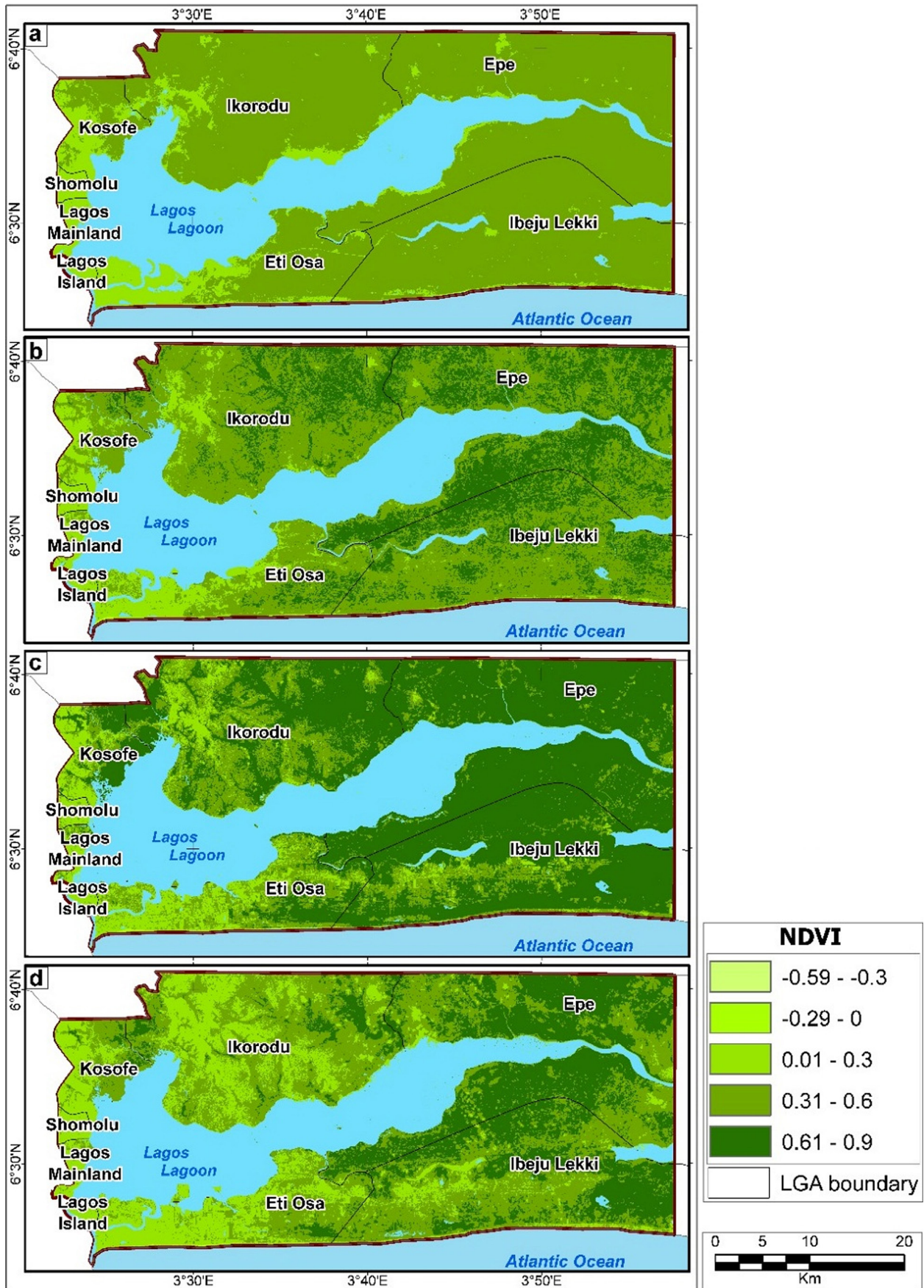


Fig. 6. Spatial pattern of NDVI for 1984 (a), 2002 (b), 2013 (c) and 2019 (d).

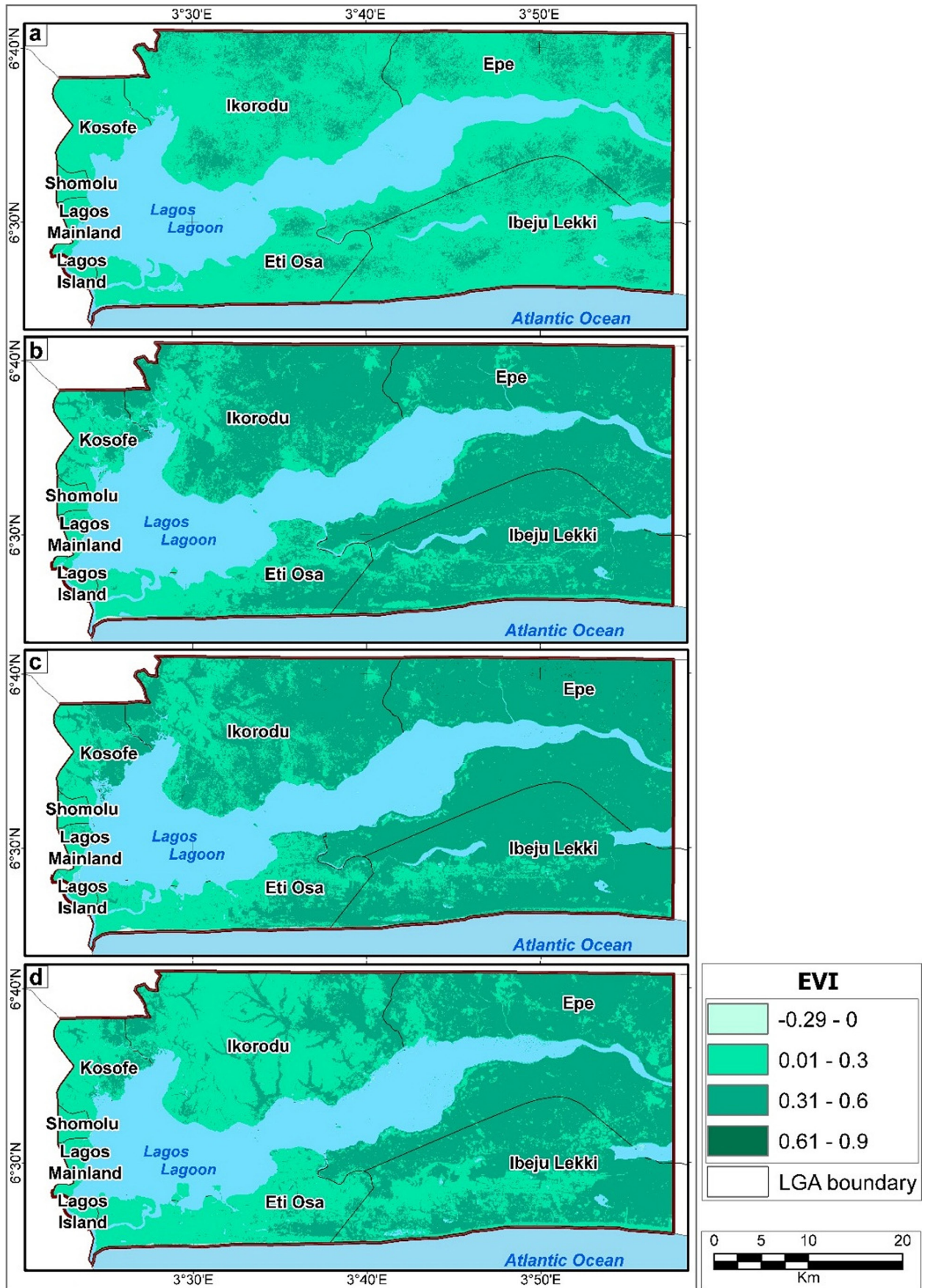


Fig. 7. Spatial pattern of EVI for 1984 (a), 2002 (b), 2013 (c) and 2019 (d).

NDVIs and EVIs. Also, where high LSTs are observed, NDVI diminishes due to variations in vegetation state or abundance.

Table 9 presents the coefficients of correlation derived from the analysis. In all the pairs of comparisons, levels of correlation were detected at the 0.01 level (2-tailed). Generally, a strong inverse relationship was observed between the

NDVI and LST and between EVI and LST. An inverse relationship between NDVI and LST was also noted in studies by Li et al. (2010), Ferrelli et al. (2018), Mukherjee and Singh (2020) and Guha et al. (2020). The strongest positive correlations were observed between NDVI and EVI over the 35-year data span. This means that the LST increased as the NDVI and EVI decreased over

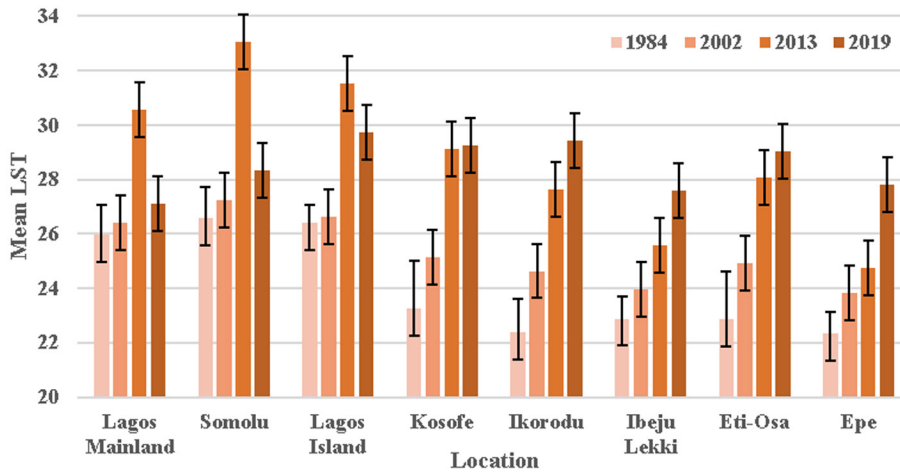


Fig. 8. Mean LSTs (°C) associated with the eight LGAs.

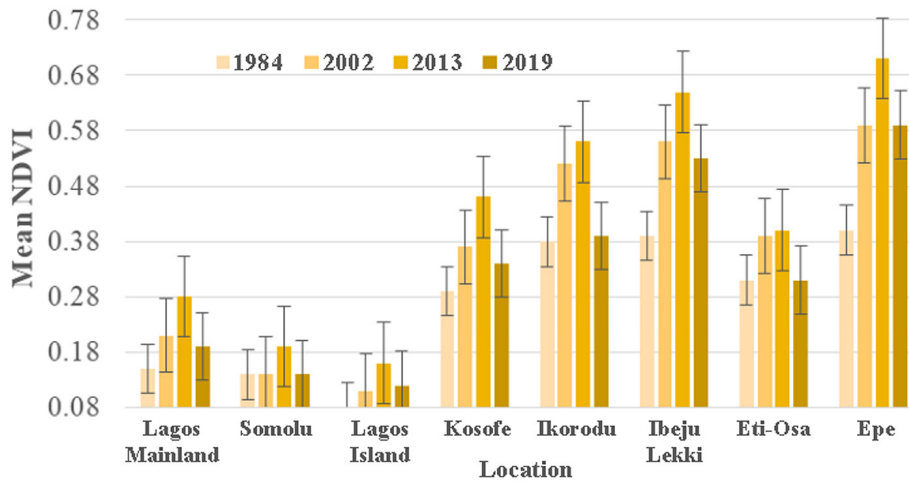


Fig. 9. Mean NDVIs associated with the eight LGAs.

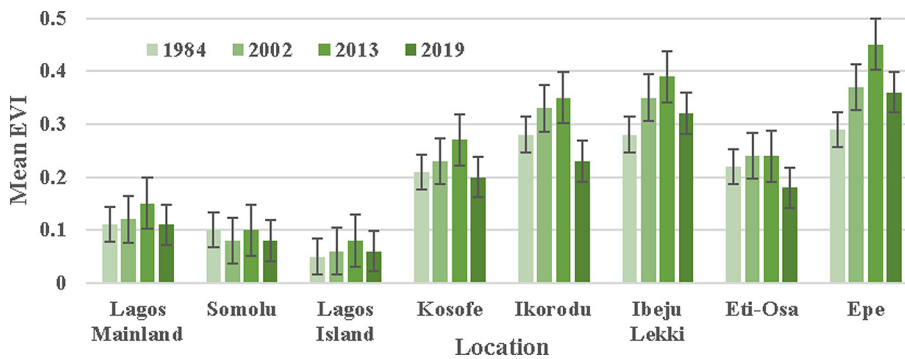


Fig. 10. Mean EVIs associated with the eight LGAs.

Table 9. Coefficient of correlation (*r*) between LST, NDVI and ENVI in years 1984, 2002, 2013 and 2019.

Parameter	LST				NDVI				EVI			
	1984	2002	2013	2019	1984	2002	2013	2019	1984	2002	2013	2019
LST 1984	1.00	0.62	0.53	0.31	-0.63	-0.62	-0.51	-0.46	-0.63	-0.60	-0.48	-0.45
LST 2002	0.62	1.00	0.80	0.60	-0.48	-0.70	-0.68	-0.71	-0.42	-0.65	-0.58	-0.69
LST 2013	0.53	0.80	1.00	0.66	-0.54	-0.75	-0.86	-0.85	-0.48	-0.69	-0.79	-0.85
LST 2019	0.31	0.60	0.66	1.00	-0.16	-0.41	-0.53	-0.64	-0.13	-0.37	-0.43	-0.62
NDVI 1984	-0.63	-0.48	-0.54	-0.16	1.00	0.80	0.63	0.53	0.99	0.78	0.66	0.56
NDVI 2002	-0.62	-0.70	-0.75	-0.41	0.80	1.00	0.82	0.73	0.77	0.98	0.80	0.74
NDVI 2013	-0.51	-0.68	-0.86	-0.53	0.63	0.82	1.00	0.86	0.58	0.78	0.96	0.86
NDVI 2019	-0.46	-0.71	-0.85	-0.64	0.53	0.73	0.86	1.00	0.47	0.68	0.79	0.96
EVI 1984	-0.63	-0.42	-0.48	-0.13	0.99	0.77	0.58	0.47	1.00	0.75	0.63	0.51
EVI 2002	-0.60	-0.65	-0.69	-0.37	0.78	0.98	0.78	0.68	0.75	1.00	0.78	0.71
EVI 2013	-0.48	-0.58	-0.79	-0.43	0.66	0.80	0.96	0.79	0.63	0.78	1.00	0.82
EVI 2019	-0.45	-0.69	-0.85	-0.62	0.56	0.74	0.86	0.96	0.51	0.71	0.82	1.00

Table 10. Linear regression analysis between the LST, NDVI, EVI and the time period, T.

Land cover class	Equation	R ²	Significance (p<0.001)	Sampled cells
All land cover classes	LST = 0.193T - 8.542NDVI - 356.929	0.812	0.000	667784
	LST = 0.173T - 12.441EVI - 316.797	0.784	0.000	
Bare land	LST = 0.158T - 6.072EVI - 288.905	0.542	0.000	10865
	LST = 0.158T - 4.395NDVI - 289.447	0.557	0.000	
Built-up area	LST = 0.149T - 7.863EVI - 269.420	0.410	0.000	123246
	LST = 0.153T - 5.335NDVI - 276.318	0.421	0.000	
Vegetation	LST = 0.159T - 9.795EVI - 290.462	0.729	0.000	533673
	LST = 0.187T - 7.943NDVI - 344.852	0.770	0.000	

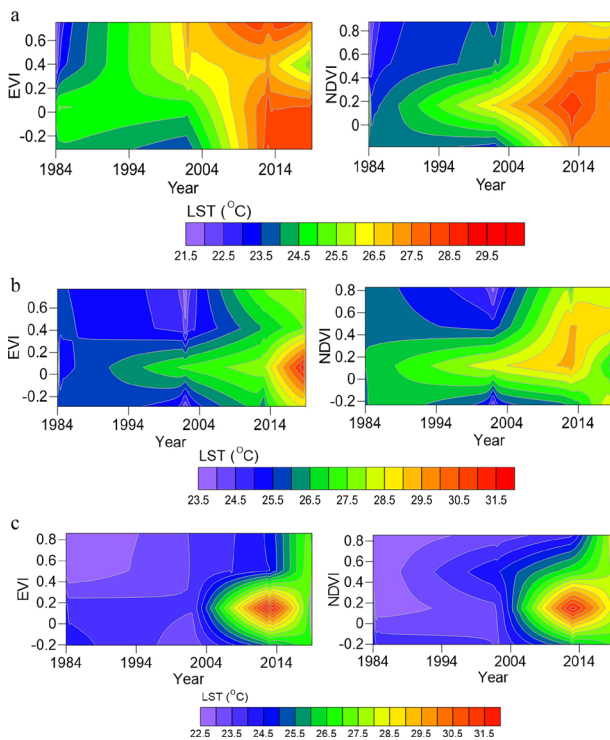


Fig. 11. Temporal relationship between EVI and NDVI and LST in bare land class (a), in built-up area class (b) and in vegetation class (c).

time. However, the value of the coefficient of correlation (*r*) decreases from 1984 to 2019 (*r* values shown in bold). This implies that although high positive *r* was obtained, the VI around the lagoon environment is decreasing yearly, inferred from the gentle gradient of *r* from 1984 to 2019.

The regression analysis between the parameters and the time period presented in Table 10 shows a negative linear relationship between the LST and the VIs over the years. Several authors have also noted this inverse relationship, for example, Dewan and Corner (2012), Ferrelli et al. (2015), Guha et al. (2020) and Mukherjee and Singh (2020). This means that the LST increased as the NDVI and EVI decreased over time. The linear models show the existence of significant relationships between the VIs and the LST. In consonance with the submission of Ferreira and Duarte (2019), the R² shows that the NDVI has a better fit and relationship with LST. The relationship between the LST, NDVI and EVI in vegetation cover shows a better fit than the bare land and built-up areas with R² values as follows: vegetation: (0.729, 0.770), bare land (0.542, 0.557) and

built-up area (0.410, 0.421). This shows the homogeneity in the relationship between the LST and the VIs in the vegetation class. Figure 11 shows the graphical representation of the relationship between the LST, NDVI and EVI across the years. Figure 11a shows the heterogeneous distribution of the LST over the years with respect to the VIs (NDVI and EVI) in bare land. Between the years 2014 and 2019, high LST values 27.5–28.5°C have moderate NDVI and EVI values between -0.2 and 0.6. Figure 11b shows a less heterogeneous distribution of the LST over the years with respect to the VIs (NDVI and EVI) in built-up area. Between the years 2014 and 2019, high LST values (29–30°C) have moderate NDVI and EVI values between -0.2 and 0.2. Figure 11c shows a homogenous distribution of the LST over the years with respect to the VIs (NDVI and EVI) in vegetation. Between the years 2014 and 2019, high LST values (29–30°C) have moderate NDVI and EVI values between -0.2 and 0.2.

Analysis of CI

Table 11 presents the CI calculated for bare land, built-up area and vegetation. The analysis suggests that the increasing LSTs are largely attributable to the built-up areas due to the highest CIs of 0.08 in 1984, 0.14 in 2002, 0.67 in 2013 and 0.35 in 2019. Conversely, vegetation had a cooling influence and negative contribution to LST as evident in the CIs of -0.10 in 1984, -0.19 in 2002, -0.68 in 2013 and -0.36 in 2019. The cooling influence of the vegetation is increasing over time while the warming influence of built-up areas is also increasing.

In 2013, vegetation recorded its highest cooling influence. However, between 1984 and 2002 there was no significant cooling influence of vegetation on the LST. This is confirmed by the depletion of vegetation in the lagoon environment within the same period. Remarkably, while the CI value for vegetation was declining from 2003, that of built-up areas was increasing (Fig. 12). This indicates

that the cooling influence of vegetation reached its maximum in 2013 before it started declining. However, that of the built-up area followed the opposite trend. This implies that the cooling effect of the vegetation was very high between 2003 and 2013 in the vegetation-covered areas but very low in the built-up areas. Possibly this could be a result of the tree greening programmes enforced by the Lagos State Government to create more green areas by planting trees and expanding the green environment in Lagos State generally (Adegboye 2013, Soladoye, Oromakinde 2013). The 2013 tree planting campaign was the fifth anniversary of tree planting initiated by the state government since 2008. A possible explanation for the reduction in built-up area CI between 2013 and 2019 is the influence of sea breeze which conditions the climates of coastal urban areas, leading to incidence of low temperatures in coastal areas (Ferrelli et al. 2018). Interestingly, a point of intersection was observed (Fig. 12) in

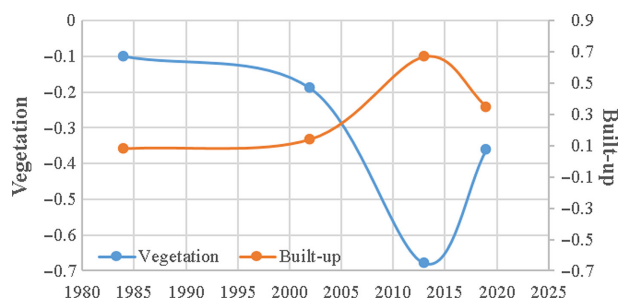


Fig. 12. CI plot of vegetation against built-up areas between 1984 and 2019.

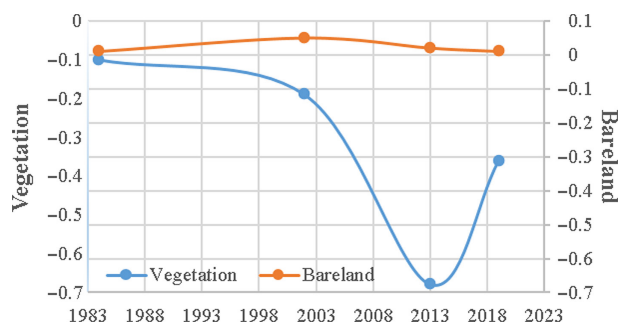


Fig. 13. CI plot of vegetation against bare land between 1984 and 2019.

Table 11. Contribution index (CI).

Land Cover	1984			2002			2013			2019		
	Dt [°C]	S	CI									
Bare Land	2.63	0.00	0.01	1.72	0.03	0.05	2.34	0.01	0.02	0.77	0.01	0.01
Built-up Area	3.71	0.02	0.08	1.91	0.07	0.14	2.88	0.23	0.67	1.40	0.25	0.35
Vegetation	-0.13	0.74	-0.10	-0.28	0.67	-0.19	-1.26	0.54	-0.68	-0.68	0.52	-0.36

2005 with CI value of approximately -0.3 and 0.2 for vegetation and built-up area, respectively. This proposes a critical point of decision because in 2019 the same value is almost becoming the intersection point. This needs to be further investigated to initiate a decision plan for positive action in the lagoon environment.

Conversely, the relationship between the CI value of vegetation and bare land shows that bare land had almost no significant contribution to the cooling effect in the study area (Fig. 13). However, in 2003 while the cooling effect by the vegetation began to increase, that of bare land was decreasing very slowly until it reached a peak of zero in 2019.

Trend Analysis

Table 12 presents the mean LST, NDVI and EVI across the years, which were variables in

the trend analysis. At 90% confidence interval, i.e. p -value = 0.10 , there is a significant upward trend in the LST values over the years across the study area with the Mann-Kendall statistic (S) of 6 and significance value lower than 0.10 . Further trend analysis was carried out for individual land cover classes. The parameters LST, NDVI and EVI appear to have an upward trend in the bare land class with S value of 6 and significance value 0.042 . The LST, NDVI and EVI do not follow an upward trend across the years for built-up areas. The LST follows an upward trend across the years in the vegetated area but not the NDVI and EVI. Sen's estimate of slope (Q_{med}) shows that the mean LST increases by 0.178°C annually in the Lagos Lagoon environment. When considered on a land cover class basis, the bare land mean LST increases by $0.115^{\circ}\text{C a}^{-1}$, the mean NDVI and mean EVI by 0.006 a^{-1} and 0.003 a^{-1} , respectively.

Table 12. Trend Analysis using the Mann-Kendall test.

Category	Time	Mean LST [$^{\circ}\text{C}$]	Mean NDVI [-]	Mean EVI [-]
All land cover classes	1984	22.68	0.37	0.27
	2002	24.34	0.52	0.32
	2013	26.46	0.60	0.37
	2019	28.4	0.47	0.28
	S	6	2	2
	Sig.	0.042*	0.375	0.375
	Q_{med}	0.178	-	-
Bare land	1984	25.31	0.13	0.10
	2002	26.06	0.25	0.16
	2013	28.80	0.25	0.18
	2019	29.17	0.29	0.19
	S	6	6	6
	Sig.	0.042*	0.042*	0.042*
	Q_{med}	0.115	0.006	0.003
Built-up area	1984	26.39	0.14	0.10
	2002	26.25	0.26	0.16
	2013	29.34	0.37	0.23
	2019	29.80	0.27	0.16
	S	4	4	3
	Sig.	0.167	0.167	0.375
	Q_{med}	-	-	-
Vegetation	1984	22.55	0.38	0.27
	2002	24.06	0.56	0.35
	2013	25.20	0.70	0.43
	2019	27.72	0.56	0.34
	S	6	4	2
	Sig.	0.042*	0.167	0.375
	Q_{med}	0.126	-	-

Conclusions

The results from this study reveal wide spatial variability in the Lagos Lagoon environment, the system has changed considerably from an environment dominated by natural vegetation of about 74.05% of the study area in 1984 suddenly to 52.32% in 2019. The environment surrounding the lagoon has largely and rapidly transformed from a vegetation dominated system to one sprawling with urban areas. This inference is in agreement with the submission of Ji et al. (2001), who confirmed that such changes are a common occurrence where urban development occurs with the depletion of the natural ecosystem. Hence, the rate of urban expansion aligns with the depletion of the natural vegetation, which is area-dependent. It was found that the vegetation in the study area has declined from 1321.78 km^2 to 933.83 km^2 between 1984 and 2019 at an annual declining rate of $11.08 \text{ km}^2 \text{ a}^{-1}$. Within the same period, the built-up areas increased from 40.77 km^2 to 441.49 km^2 , at an annual increasing rate of $11.44 \text{ km}^2 \text{ a}^{-1}$. Regarding the spatial distribution of NDVI, an increase in vegetation greenness (consistent and most likely positive trends) was mostly observed in 2013 along Ibeju Lekki, Epe and part of Ikorodu. This increase in the photosynthetic activity agrees with the global general

trend observed due to the increase in forested areas, increased atmospheric nitrogen deposition, the juvenile age structure, CO₂ fertilisation and climate change (Luyssaert et al. 2010). NDVI increases along the three areas mentioned above could be aligned with the constant release of water from upland dams such as the Oyan dam in Ogun State which flow to cover most of these areas and nourish the environment for increased productivity. A huge decrease in NDVI was experienced in 2019 along Shomolu, Lagos Island and Lagos Mainland, and the trend spreads to Kosofe, Ikorodu and Eti-Osa. This might be related to urban expansion and destruction of the green areas in the struggle to get spaces for stalls by the small-scale business enterprises.

It was observed that the built-up areas were the major contributor to the warming of the ecosystem whereas the areas of vegetation had a cooling effect. This confirms the influence of vegetation and natural cover in mitigating the intensity and spread of UHIs. The inference from the results of LST in LGAs such as Lagos Island, Somolu, Kosofe and Lagos Mainland justified the high rate of urban heat that is being experienced in these areas. The present results of the land cover investigation around the Lagos Lagoon environment are also suggestive of reductions in habitat availability. These are not enough to assess the damage or the impact on a holistic system, even though there is evidence that some areas appear not to have a visible effect in terms of vegetation disappearance. However, it does not indicate that there was no change even though such changes might be very small. Future research should integrate the method in this study with ecological factors for a very robust investigation to capture temporal changes. Consequently, to reduce the extent of the disappearance of the coastal environments in the area to natural causes, some measures must be administered such as buffer areas for regional coastal reserves in Nigeria coastal zone as suggested for the United States of America in Luque (2000). This will help in considering ways of recovering and preserving the natural vegetation since retaining biodiversity aesthetic values and water quality are as important as providing services for human development. Finally, the government needs to plan green areas that will serve to cushion the effect of the increased urban heat.

Acknowledgements

The authors are grateful to the USGS for access to the Landsat imageries and the USGS EROS Centre for the Landsat spectral indices used in this research. Also, credits are due to the team that conducted the original research on the Landsat surface reflectance products (Masek et al. 2006, Vermote et al. 2016). The authors also thank the Department of Surveying and Geoinformatics at the University of Lagos for providing a conducive research environment within which the study was conducted. We also thank the editor and anonymous reviewers of this journal for their feedback which helped to improve the quality of the paper. This research did not receive any specific grant from funding agencies in the public, commercial or not-for-profit sectors.

Authors' contributions

Conceptualisation and design: ASA, CJO; acquisition of data: ASA, CJO, ROA; data analysis and interpretation: ASA, CJO, OED, ROA, TJS; manuscript writing and revision: ASA, CJO, OED, ROA, TJS.

References

- Abbas I.L., 2008. Use of satellite remote sensing and geographic information systems to monitor land degradation along Ondo Coastal Zone (Nigeria). *Balwois, Orid, Macedonia* 27: 1-13.
- Abbas I.L., Fasona M.J., 2012. Remote sensing and geographic information techniques: Veritable tools for land degradation assessment. *American Journal of Geographic Information System* 1(1): 1-6.
- Aboelnour M., Engel B., 2018. Application of remote sensing techniques and geographic information systems to analyze land surface temperature in response to land use/land cover change in Greater Cairo Region, Egypt. *Journal of Geographic Information System* 10: 57-88. DOI 10.4236/jgis.2018.101003.
- Adegboye K., 2013. Fashola highlights importance of greenery at 2013 tree planting campaign—Vanguard News. Vanguard Newspaper. Online: <https://www.vanguardngr.com/2013/07/fashola-highlights-importance-of-greenery-at-2013-tree-planting-campaign/> (accessed 20 August 2020).
- Adegun O., Odunuga S., Appia Y., 2015. Dynamics in the landscape and ecological services in system I drainage area of Lagos. *Ghana Journal of Geography* 7(1): 75-96.
- Ajibola M., Adeleke A.M., Ogungbemi A., 2016. An assessment of wetland loss in Lagos Metropolis, Nigeria. *Developing Country Studies* 6(7): 1-7.

- Ajibola M., Adewale B., Ijase K., 2012. Effects of urbanisation on Lagos wetlands. *International Journal of Business and Social Science* 3(17): 310–318.
- Akpootu D.O., Iliyasu M.I., Mustapha W., Aruna S., Yusuf S.O., 2017. The influence of meteorological parameters on atmospheric visibility over Ikeja, Nigeria. *Archives of Current Research International* 9(3): 1–12, Article no. ACRI.36010
- Anderson J.R., 1971. Land use classification schemes used in selected recent geographic applications of remote sensing. *Photogrammetric Engineering* 37(4): 379–387.
- Aribisala J.O., Ogundipe O.M., Akinkulore O.O., 2016. The study of climate change. *British Journal of Applied Science and Technology* 13(6): 1–7.
- Boegh E., Soegaard H., Broge N., Hasager C.B., Jensen N.O., Schelde K., et al., 2002. Airborne multispectral data for quantifying leaf area index, nitrogen concentration, and photosynthetic efficiency in agriculture. *Remote Sensing of Environment* 81: 179–193.
- Bolstad P., Lillesand T.M., 1991. Rapid maximum likelihood classification. *Photogrammetric Engineering and Remote Sensing* 57(1): 67–74.
- Brendel A.S., Ferrelli F., Piccolo M.C., Perillo G.M.E., 2019. Assessment of the effectiveness of supervised and unsupervised methods: Maximizing land-cover classification accuracy with spectral indices data. *Journal of Applied Remote Sensing* 13(1): 014503. DOI 10.1117/1.JRS.13.014503.
- Butuc B.R., Moldovean G., 2011. Environmental impact scenario of an azimuthal tracked PV platform based on CO2 emissions reduction. *Environmental Engineering and Management Journal* 10: 271–276.
- Chen P., Fedosejevs G., Tiscareño-López M., Arnold, J. G., 2006b. Assessment of MODIS-EVI, MODIS-NDVI and vegetation-NDVI composite data using agricultural measurements: An example at corn fields in Western Mexico. *Environmental Monitoring and Assessment* 119: 69–82. DOI 10.1007/s10661-005-9006-7.
- Chen X-L., Zhao H-M., Li P.-X., Yin Z.-Y., 2006a. Remote sensing image based analysis of the relationship between urban heat island and land use/cover changes. *Remote Sensing of Environment* 104: 133–146.
- David A.R., 2008. A re-interpretation of Landsat TM data on Chernobyl. *International Journal of Remote Sensing* 10(8): 1423–1427.
- Deng Y., Wang S., Bai X., Tian Y., Wu L., Xiao J., Chen F., Qian Q., 2018. Relationship among land surface temperature and LUCC, NDVI in typical karst area. *Scientific Reports* 8(1): 1–12. DOI 10.1038/s41598-017-19088-x.
- Dewan A.M., Corner, R.J., 2012. The impact of land use and land cover changes on land surface temperature in a rapidly urbanizing megacity. In: *IGARSS, Munich, Germany, 22–27 July 2012*; pp. 6337–6339.
- Farina A., 2012. Exploring the relationship between land surface temperature and vegetation abundance for urban heat island mitigation in Seville, Spain. M.Sc. Thesis, Lund University.
- Fasona M., Omojola A., Odunuga S., Tejuoso O., Amogu N., 2005. An appraisal of sustainable water management solutions for large cities in developing countries through GIS: The case of Lagos, Nigeria. In: *Proceeding of the Symposium S2 Held during the 7th IAHS Scientific Assembly, Foz do Iguacu, Brazil, 3–9 April 2005*; pp. 49–57.
- Ferreira L.S., Duarte D.H.S., 2019. Exploring the relationship between urban form, land surface temperature and vegetation indices in a subtropical megacity. *Urban Climate* 27: 105–123.
- Ferrelli F., Bustos M., Huamantínco-Cisneros M., Piccolo M., 2015. Utilization of satellite images to study the thermal distribution in different soil covers in Bahía Blanca city (Argentina). *Revista de Teledetección* 44: 31–42.
- Ferrelli F., Cisneros M.A.H., Delgado A.L., Piccolo M.C., 2018. Spatial and temporal analysis of the LST-NDVI relationship for the study of land cover changes and their contribution to urban planning in Monte Hermoso, Argentina. *Documents d'Anàlisi Geogràfica* 2018, 64/1: 25–47. DOI 10.5565/rev/dag.355
- Gao X., Huete A.R., Didan K., 2003. Multisensor comparisons and validation of MODIS vegetation indices at the semi-arid Jornada experimental range. *IEEE Transactions on Geoscience and Remote Sensing* 41: 2368–2381.
- Gao X., Huete A.R., Ni W., Miura T., 2000. Optical-biophysical relationships of vegetation spectra without background contamination. *Remote Sensing of Environment*, 74: 609–620.
- Ghulam A., 2010. Calculating surface temperature using landsat thermal imagery. Online: https://serc.carleton.edu/files/NAGTWorkshops/gis/activities2/student_handout_calculating_te.pdf (accessed 25 March 2016).
- Gilbert R.O., 1987. Statistical methods for environmental pollution monitoring. Van Nostrand Reinhold Company Inc., New York.
- Gocic M., Trajkovic S., 2013. Analysis of changes in meteorological variables using Mann-Kendall and Sen's slope estimator statistical tests in Serbia. *Global and Planetary Change* 100: 172–182.
- Green E., Mumby P., Edwards A., Clark C., 1996. A review of remote sensing for the assessment and management of tropical coastal resources. *Coastal Management* 24(1): 1–40.
- Guha S., Govil H., Dey A., Gill N., 2020. A case study on the relationship between land surface temperature and land surface indices in Raipur City, India. *Geografisk Tidsskrift-Danish Journal of Geography* 120(1): 35–50. DOI 10.1080/00167223.2020.1752272.
- Gutman G., Huang C., Chander G., Noojipady P., Masek J. G., 2013. Assessment of the NASA-USGS global land survey (GLS) datasets. *Remote Sensing of Environment* 134: 249–265.
- Hamed K.H., 2008. Trend detection in hydrologic data: The Mann-Kendall trend test under the scaling hypothesis. *Journal of Hydrology* 349(3–4): 350–363. DOI 10.1016/j.jhydrol.2007.11.009
- Hamoodi M.N., Corner R., Dewan A., 2019. Thermophysical behaviour of LULC surfaces and their effect on the urban thermal environment. *Journal of Spatial Science* 64(1): 111–130. DOI 10.1080/14498596.2017.1386598
- Hasmadi M., Pakhriyazad H.Z., Shahrin M.F., 2009. Evaluating supervised and unsupervised techniques for land cover mapping using remote sensing data. *Geografika: Malaysian Journal of Society and Space* 5(1): 1–10.
- Hoek van Dijke A.J., Mallick K., Teuling A.J., Schlerf M., Machwitz M., Hassler S.K., Blume T., Herold M., 2019. Does the normalized difference vegetation index explain spatial and temporal variability in sap velocity in temperate forest ecosystems? *Hydrology and Earth System Sciences* 23: 2077–2091. DOI 10.5194/hess-23-2077-2019.
- Hou G.L., Zhang H.Y., Wang Y.Q., Qiao Z.H., Zhang Z.X., 2010. Retrieval and spatial distribution of land surface temperature in the middle part of Jilin province based on MODIS data. *Scientia Geographica Sinica* 30, 421–427.

- Huete A.R., 1988. A soil adjusted vegetation index (SAVI). *Remote Sensing of Environment* 25, 295–309.
- Huete A.R., Didan K., Miura T., Rodriguez E.P., Gao X., Ferreira L.G., 2002. Overview of the radiometric and biophysical performance of the MODIS Vegetation indices'. *Remote Sensing of Environment* 83: 195–213.
- Huete A.R., Justice C., Van Leeuwen W., 1999. MODIS vegetation index (MOD13). Algorithm Theoretical Basis Document. Version 3.
- James G.K., Adegoke J.O., Saba E., Nwilo P., Akinyede, J., 2007. Satellite-based assessment of the extent and changes in the mangrove ecosystem of the Niger Delta. *Marine Geodesy* 30(3), 249–267.
- Jeevalakshmi D., Narayana Reddy S., Manikiam B., 2017. Land surface temperature retrieval from Landsat data using Emissivity Estimation. *International Journal of Applied Engineering Research* 12(20): 9679–9687.
- Ji C., Liu Q., Sun D., Wang S., Lin P., Li X., 2001. Monitoring urban expansion with remote sensing in China. *International Journal of Remote Sensing* 22(8): 1441–1455.
- Jimenez-Munoz J.C., Sobrino J.A., 2003. A generalized single-channel method for retrieving land surface temperature from remote sensing data. *Journal of Geophysical Research* 108, DOI 10.1029/2003JD003480.
- Kaufmann R.K., Seto K.C., Shneider A., Liu Z., Zhou L., Wang W., 2007. Climate response to rapid urban growth: Evidence of human-induced precipitation deficit. *Journal of Climate* 20: 2299–2306. DOI 10.1175/JCLI4109.1
- Kindscher K., Fraser A., Jakubauskas M., Debinski D., 1997. Identifying wetland meadows in Grand Teton National Park using remote sensing and average wetland values. *Wetlands Ecology and Management* 5(4): 265–273. DOI 10.1023/A:1008265324575.
- Kolios S., Stylios C.D., 2013. Identification of land cover/land use changes in the greater area of the Preveza peninsula in Greece using Landsat satellite data. *Applied Geography* 40: 150–160.
- Li W.F., Cao Q.W., Kun L., Wu J.S., 2017. Linking potential heat source and sink to urban heat island: Heterogeneous effects of landscape pattern on land surface temperature. *Science of the Total Environment* 586: 457–465.
- Li Z., Li X., Wei D., Xu X., Wang H., 2010. An assessment of correlation on MODIS-NDVI and EVI with natural vegetation coverage in Northern Hebei Province, China. *Procedia Environmental Sciences* 2: 964–969.
- Luque S., 2000. Evaluating temporal changes using multi-spectral scanner and thematic Mapper data on the landscape of a natural reserve: The New Jersey Pine Barrens, a case study. *International Journal of Remote Sensing* 21(13–14): 2589–2610.
- Luyssaert S., Ciais P., Piao S.L., Schulze E.D., Jung M., Zaehle S., et al., 2010. The European Carbon Balance: Part 3: Forests. *Global Change Biology* 2010. DOI 10.1111/j.1365-2486.2009.02056.x.
- Malik M.S., Shukla J.P., Mishra S., 2019. Relationship of LST, NDBI and NDVI using Landsat-8 data in Kandaihimmat Watershed, Hoshangabad, India. *Indian Journal of Geo Marine Sciences* 48(1): 25–31.
- Masek J.G., Vermote E.F., Saleous N.E., Wolfe R., Hall F.G., Huemmrich K.F., Gao F., Kutler J., Lim T.-K., 2006. A Landsat surface reflectance data set for North America, 1990–100. *IEEE Geoscience and Remote Sensing Letters* 3: 68–72.
- Matsushita B., Yang W., Chen J., Onda Y., Qiu G., 2007. Sensitivity of the Enhanced Vegetation Index (EVI) and Normalized Difference Vegetation Index (NDVI) to topographic effects: A case study in high-density Cypress forest. *Sensors* 2007(7): 2636–2651.
- Meera G.G., Parthiban S., Nagaraj T., Christy A., 2015. NDVI: Vegetation change detection using remote sensing and GIS – A case study of Vellore District. 3rd International Conference on Recent Trends in Computing 2015 (ICRTC-2015). *Procedia Computer Science* 57(2015): 1199–1210. DOI 10.1016/j.procs.2015.07.415.
- Mildrexler D.J., Zhao M., Heinsch F.A., Running S.W., 2007. A new satellite-based methodology for continental-scale disturbance detection. *Ecological Applications* 17(1): 235–250.
- Mildrexler D.J., Zhao M., Running S.W., 2009. Testing a MODIS global disturbance index across North America. *Remote Sensing of Environment* 113(10): 2103–2117.
- Mukherjee F., Singh D., 2020. Assessing land use–land cover change and its impact on land surface temperature using LANDSAT data: A comparison of two urban areas in India. *Earth Systems and Environment* 4, 385–407. DOI 10.1007/s41748-020-00155-9.
- Mushtaq A.G., Asima, N., 2016. Determining the Vegetation Indices (NDVI) from landsat 8 satellite data. Article DOI 10.21474/IJAR01/1348. *International Journal of Advance Research* 4(8): 1459–1463. DOI 10.21474/IJAR01/1348
- Ngie A., Abutaleb K., Ahmed F., Taiwo O.J., Darwish A.A., Ahmed M., 2016. An estimation of land surface temperatures from landsat ETM+ images for Durban, South Africa. *Rwanda Journal* 1(1): 17p. DOI: 10.4314/rj.v1i25.2D.
- Nwilo P.C., Ayodele E.G., Okolie C.J., Orji M.J., Marve M.F., Oyelade E.A., et al., 2020. An assessment of seasonal variations in the CREF CORS at the University of Lagos. *Geomatics, Landmanagement and Landscape* No. 1, 2020: 63–77. DOI 10.15576/GLL/2020.1.63.
- Nwilo P.C., Olayinka D.N., Atagbaza A.O., Adzandeh A.E., 2012. Determination of Land Surface Temperature (LST) and potential urban heat Island effect in parts of Lagos state using satellite imageries. *FUTY Journal of the Environment* 7(1): 19–33. DOI 10.4314/fje.v7i1.2.
- Obiefuna J.N., Nwilo P.C., Atagbaza A.O., Okolie C.J., 2013a. Spatial Changes in the Wetlands of Lagos/Lekki Lagoons of Lagos, Nigeria. *Journal of Sustainable Development* 6(7): 123–133. DOI 10.5539/jsd.v6n7p123.
- Obiefuna J.N., Nwilo P.C., Atagbaza A.O., Okolie C.J., 2013b. Land Cover Dynamics Associated with the Spatial Changes in the Wetlands of Lagos/Lekki Lagoon System of Lagos, Nigeria. *Journal of Coastal Research* 29(3): 671–679. DOI 10.2112/JCOASTRES-D-12-00038.1.
- Obiefuna J.N., Nwilo P.C., Okolie C.J., Emmanuel E.I., Dar-amola O.E., 2018. Dynamics of land surface temperature in response to land cover changes in Lagos metropolis. *Nigerian Journal of Environmental Sciences and Technology* 2(2): 148–159. DOI 10.36263/nijest.2018.02.0074.
- Odindi J.O., Bangamwabo V., Mutanga O., 2015. Assessing the value of urban green spaces in mitigating multi-seasonal urban heat using MODIS Land Surface Temperature (LST) and landsat 8 data. *International Journal of Environmental Research* 9(1): 9–18.
- Odindi J.O., Mutanga O., Abdel-Rahman E.M., Adam E., Bangamwabo V., 2017. Determination of urban land-cover types and their implication on thermal characteristics in three South African coastal metropolitans using remotely sensed data. *South African Geographical Journal* 99: 52–67.

- Odunuga S., Oyebande L., 2007. Change detection and hydrological implications in the Lower Ogun flood plain, SW Nigeria. *Remote Sensing for Environmental Monitoring and Change Detection, IAHS-AISH Publications* 316: 91–99.
- Oguz H., 2013. LST calculator: A program for retrieving land surface temperature from Landsat TM/ETM+ imagery. *Environmental Engineering and Management Journal* 12(3): 549–555.
- Ojeh V.N., Balogun A.A., Okhimamhe A.A., 2016. Urban-rural temperature differences in Lagos. *Climate* 4: 29. DOI 10.3390/cli4020029.
- Panda U., Mohanty, P., 2008. Monitoring and modelling of Chilika environment using remote sensing data. *Proceedings of Taal 2007: The 12th World Lake Conference*: 617–638.
- Panigrahi S., Acharya B.C., Panigrahy R.C., Nayak B.K., Banarjee K., Sarkar S.K., 2007. Anthropogenic impact on water quality of Chilika lagoon RAMSAR site: A statistical approach. *Wetlands Ecology and Management* 15(2): 113–126.
- Phompila C., Lewis M., Ostendorf B., Clarke K., 2015. MODIS EVI and LST temporal response for discrimination of tropical land covers. *Remote Sensing* 7(5): 6026–6040.
- Qiu J., Yang J., Wang Y., Su H., 2018. A comparison of NDVI and EVI in the DisTrad model for thermal sub-pixel mapping in densely vegetated areas: A case study in Southern China. *International Journal of Remote Sensing* 39(8): 2105–2118. DOI 10.1080/01431161.2017.1420929.
- Rankine C., Sánchez-Azofeifa G.A., AntonioGuzmán J., Espirito-Santo M.M., Sharp I., 2017. Comparing MODIS and near-surface vegetation indexes for monitoring tropical dry forest phenology along a successional gradient using optical phenology towers. *Environmental Research Letters* 12(2017): 105007. DOI 10.1088/1748-9326/aa838c
- Roth M., 2008. Urban climate considerations for the development of sustainable cities. In: *Proceedings for Recent Findings on Planning and Designing Sustainable Cities, Singapore*, November 2008. National University of Singapore.
- Salau O.R., Fasuba A., Aduloju K.A., Adesakin G.E., Fatigun A.T., 2016. Effects of changes in ENSO on temperature and rainfall distribution in Nigeria. *Climate* 2016, 4(1): 1–12. DOI 10.3390/cli4010005.
- Schott J.R., Volchok W.J., 1985. Thematic Mapper thermal infrared calibration. *Photogrammetric Engineering and Remote Sensing* 51: 1351–1357.
- Semeraro T., Luvisi A., Lillo A.O., Aretano R., Buccolieri R., Marwan N., 2020. Recurrence analysis of vegetation indices for highlighting the ecosystem response to drought events: An application to the Amazon forest. *Remote Sensing* 12: 907. DOI 10.3390/rs12060907
- Sen P.K., 1968. Estimates of the regression coefficient based on Kendall's tau. *Journal of the American Statistical Association* 63(324): 1379–1389.
- Sharma A., Boroevich K.A., Shigemizu D., Kamatani Y., Kubo M., Tsunoda T., 2017. Hierarchical maximum likelihood clustering approach. *IEEE Transactions on Biomedical Engineering* 64(1): 112–122.
- Sharma M., Gupta R., Kumar D., Kapoor R., 2011. Efficacious approach for satellite image classification. *Journal of Electrical and Electronics Engineering Research* 3(8): 143–150.
- Sobrino J.A., Julien Y., 2013. Trend analysis of global MODIS-Terra vegetation indices and land surface temperature between 2000 and 2011. *IEEE Journal of Selected Topics in Applied Earth Observations and Remote Sensing* 6(5): 2139–2145.
- Soladoye O., Oromakinde O.O., 2013. Assessment of Tree Planting Efforts in Lagos Island Local Government Area of Lagos State, Nigeria. *Environment and Natural Resources Research* 3(4): 12–18. DOI 10.5539/enrr.v3n4p12.
- Streutker D.R., 2003. Satellite-measured growth of the urban heat island of Houston, Texas. *Remote Sensing of Environment* 85(3): 282–289.
- Sun H., Sun X., Wang H., Li Y., Li X., 2011. Automatic target detection in high-resolution remote sensing images using spatial sparse coding bag-of-words model. *IEEE Geoscience and Remote Sensing Letters* 9(1): 109–113.
- Tarawally M., Wenbo X., Weiming H., Terence D.M., 2018. Comparative analysis of responses of land surface temperature to long-term land use/cover changes between a coastal and Inland City: A case of freetown and Bo town in Sierra Leone. *Remote Sensing* 10: 112, 18p. DOI 10.3390/rs10010112.
- Tatem A.J., Nayar A., Hay S.I., 2006. Scene selection and the use of NASA's global orthorectified Landsat dataset for land cover and land use change monitoring. *International Journal of Remote Sensing* 27(14): 3073–3078.
- Tran D.X., Pla F., Latorre-Carmona P., Myint S.W., Caetano M., Kieu H.V., 2017. Characterizing the relationship between land use land cover change and land surface temperature. *ISPRS Journal of Photogrammetry and Remote Sensing* 124: 119–132. DOI 10.1016/j.isprsjprs.2017.01.001.
- Ullah S., Tahir A.A., Akbar T.A., Hassan Q.K., Dewan A., Khan A.J., et al., 2019. Remote sensing-based quantification of the relationships between land use land cover changes and surface temperature over the Lower Himalayan Region. *Sustainability* 11: 5492. DOI 10.3390/su11195492.
- USGS [United States Geological Survey], 2015. *Landsat 8 (L8) Data Users Handbook, Version 1.0*. LSDS-1574. Department of the Interior, U.S. Geological Survey.
- USGS [United States Geological Survey], 2019. *Landsat 8 Surface Reflectance Code (LASRC) Product Guide*. Version 2.0. Online: <https://www.usgs.gov/media/files/landsat-8-collection-1-land-surface-reflectance-code-product-guide> (accessed 20 August 2020).
- USGS [United States Geological Survey], 2020. *Earth Resources Observation and Science (EROS) Center Science Processing Architecture (ESPA) on-demand interface user guide*. Release 3.0.0. Version 4.0
- Uyeda K.A., Stow D.A., Roberts D.A., Riggan P.J., 2017. Combining ground-based measurements and MODIS-based spectral vegetation indices to track biomass accumulation in post-fire chaparral. *International Journal of Remote Sensing* 38(3): 728–741. DOI 10.1080/01431161.2016.1271477.
- Vermote E., Justice C., Claverie M., Franch B., 2016. Preliminary analysis of the performance of the Landsat 8/OLI land surface reflectance product. *Remote Sensing of Environment* 185: 46–56.
- Weng Q., 2003. Fractal analysis of satellite-detected urban heat island effect. *Photogrammetric Engineering and Remote Sensing* 69(5): 555–566.
- Weng Q., Lu D., Schubring J., 2004. Estimation of land surface temperature – vegetation abundance relationship for urban heat island studies. *Remote Sensing of Environment* 89(4): 467–483.
- Wilson J.S., Clay M., Martin E., Stuckey D., Vedder-Risch K., 2003. Evaluating environmental influences of zoning in urban ecosystems with remote sensing. *Remote Sensing of Environment* 86(3): 303–321.

- WVO [World Weather Online], 2020. Lagos monthly climate averages. Online: www.worldweatheronline.com/lagos-weather-averages/lagos/ng.aspx (accessed 1 August 2020).
- Xian G., Crane, M., 2006. An analysis of urban thermal characteristics and associated land cover in Tampa Bay and Las Vegas using Landsat satellite data. *Remote Sensing of Environment* 104(2): 147–156.
- Xiao R., Ouyang Z., Zheng H., Li W., Schienke E.W., Wang X., 2007. Spatial pattern of impervious surfaces and their impacts on land surface temperature in Beijing, China. *Journal of Environmental Sciences* 19(2): 250–256.
- Xiao X., Zhang Q., Braswell B., Urbanski S., Boles S., Wofsy S., Moore III B., Ojima D., 2004. Modeling gross primary production of temperate deciduous broadleaf forest using satellite images and climate data. *Remote Sensing of Environment* 91(2): 256–270.
- Yuan X., Wang W., Cui J., Meng F., Kurban A., De Maeyer P., 2017. Vegetation changes and land surface feedbacks drive shifts in local temperatures over Central Asia. *Scientific Reports* 7(1): 1–8.
- Yue W., Xu J., Tan W., Xu L., 2007. The relationship between land surface temperature and NDVI with remote sensing: Application to Shanghai Landsat 7 ETM+ data'. *International Journal of Remote Sensing* 28(15): 3205–3226.
- Zaharaddeen I., Ibrahim I.B., Zachariah A., 2016. Estimation of land surface temperature of Kaduna metropolis, Nigeria using Landsat images. *Science World Journal* 11(3): 36–42.
- Zareie S., Khosravi H., Nasiri A., 2016. Derivation of land surface temperature from landsat thematic mapper (TM) sensor data and analysing relation between land use changes and surface temperature. *Solid Earth Discussions*: 1–15. DOI 10.5194/se-2016-22.
- Zhang J., Wang Y., Li Y., 2006. A C++ program for retrieving land surface temperature from the data of Landsat TM/ETM+ band 6. *Computers & Geosciences* 32(10): 1796–1805.
- Zhang Y., Balzter H., Liu B., Chen Y., 2016. Analyzing the impacts of urbanization and seasonal variation on land surface temperature based on subpixel fractional covers using landsat images. *IEEE Journal of Selected Topics in Applied Earth Observations and Remote Sensing* 10(4): 1344–1356.